Tectonics

RESEARCH ARTICLE
10.1029/2022TC007370

Key Points:
- Up to ~500 m of modern topography can be explained by sedimentation and flexural response in the western High Plains
- ~1,000–1,500 m of topography gained since the deposition of the Dakota Formation remains unexplained, termed *cryptic topography*
- Cryptic topography increases to the southwest, suggesting a role for magmatic depletion of upper mantle due to mid-Tertiary igneous activity

Supporting Information:

Supporting Information may be found in the online version of this article.

Correspondence to:

K. R. Bogolub,
kbogolub@mines.edu

Citation:

Bogolub, K. R., & Jones, C. H. (2022). Quantifying the cryptic topography of the High Plains. *Tectonics*, *41*, e2022TC007370. https://doi.org/10.1029/2022TC007370

Received 27 APR 2022
Accepted 30 JUL 2022

Quantifying the Cryptic Topography of the High Plains

Kyren R. Bogolub[1,2] and Craig H. Jones[1]

[1]Department of Geological Sciences, CIRES, University of Colorado Boulder, Boulder, CO, USA, [2]Colorado Geological Survey, Golden, CO, USA

Abstract The origin of the presently high topography of the High Plains of the western United States has been a topic of considerable debate. We remove the directly quantifiable effects of thrust loading and post-Early Cretaceous sedimentation to identify topography supported by subsurface means. We term this amount of unexplained topography *cryptic topography*. To determine the amount of topography that can be attributed to sedimentation, thrust loading, and the flexural response of the lithosphere, we estimate the thickness and density of the sedimentary rocks that overly the Dakota Formation from well logs. We then calculate the flexure that results from the emplacement of these rocks as well as the thrust load of the Rocky Mountains. We then subtract these effects from the present day Dakota horizon. The results of removing these effects indicate that between ~1 and 1.5 km of topography at the western edge of the High Plains is cryptic and demands some change in the deeper crust or mantle since the deposition of the Dakota Formation.

1. Introduction

In the North American Cordillera, the Colorado Plateau, Southern Rocky Mountains, Rio Grande Rift, and the High Plains (Figure 1) occupy most of one of the broadest orogeny in the world. The Cretaceous Dakota Formation is a near shoreline assemblage of sandstone, shales, and coal deposited across Colorado as the Western Interior Seaway transgressed across the gently east-sloping interior of the continent. In contrast, today, the High Plains in the central United States is a relatively smooth and undeformed yet elevated region that reaches over 2 km above sea level at the eastern base of the Rocky Mountains.

The cause and timing of this epeirogeny has yet to be satisfactorily explained. While the Southern Rockies have undergone some significant crustal shortening and thickening, the adjacent High Plains are undeformed and the Colorado Plateau to the west suffered far less shortening (Davis, 1999). The few hypotheses that directly account for the topography of the High Plains can be supplemented by consideration of the more numerous hypotheses addressing the uplift of the Colorado Plateau despite its different history (i.e., Cenozoic magmatism, a greater deformation, and faulting at the plateau's boundaries).

A brief overview of potential causes of uplift is needed to understand the approach of this paper. We here are concerned with surface uplift, which is simply the increase in mean elevation relative to some datum. Mechanisms causing surface uplift other than sedimentation will necessarily produce rock uplift. In the case of the High Plains, where sedimentation has dominated over erosion, surface uplift is the sum of rock uplift and sediment accumulation. Thus, sub-surface processes producing surface uplift will necessarily produce rock uplift, so we will often just refer to "uplift," meaning that both rock and surface uplift are present. Thinning of mantle lithosphere either by thermal erosion of lithosphere (Levandowski et al., 2018; Morgan & Swanberg, 1985; Roy et al., 2009) or mechanical removal of lithosphere (Spencer, 1996) could produce uplift. Conversely, additional crustal material entrained by basal traction could elevate the High Plains (Bird, 1984). Hydration, either of the mantle (E. Humphreys et al., 2003) or of the crust (Jones et al., 2015; Morgan, 2003), has been proposed as a means of raising the Plateau and/or High Plains. Lithospheric alteration by extraction of melt associated with the mid-Tertiary episode of magmatism could also drive uplift (Roy et al., 2004, 2005). Dynamic effects in the past (Mitrovica et al., 1989) or present (Liu & Gurnis, 2010; Moucha et al., 2008) can also result in uplift, in the former case by accumulating large amounts of sediment in a temporary basin, and in the latter by raising the region today through mantle flow.

These mechanisms producing uplift of the High Plains would be active at differing times and have a different spatial extent, suggesting one means of distinguishing among these might be to determine the geographic extent and/or timing of the creation of topography. Several hypotheses are related to the geometry of the subducting

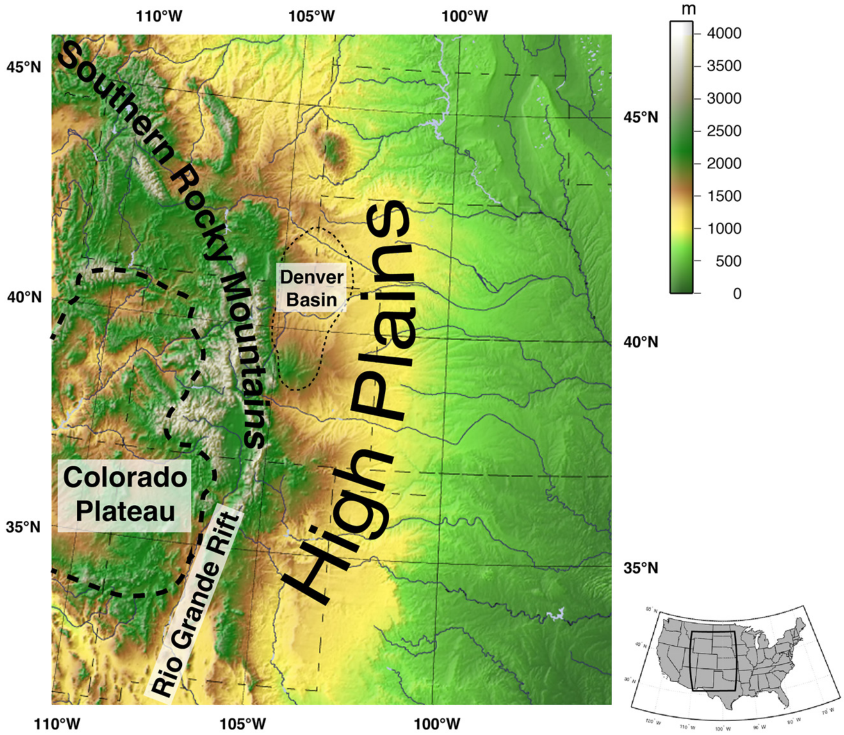

Figure 1. Location map showing the physiographic provinces discussed in the text.

Farallon slab, but they might produce uplift at different times and with different associations with a slab. Others tied to peculiarities in the structure of the lithosphere or the source of magmas will have a different spatial and temporal footprint than slab-related hypotheses.

Other factors complicate a simple comparison of modern topography to predictions from these mechanisms, and a goal of this work is to reduce such complications. In the Colorado and Kansas portion of the orogeny explored here, those elements are deposition of sediments and the loading of lithosphere by thrust faulting. The deposition of the sediments is a key element of one proposed mechanism, that of Mitrovica et al. (1989). Levandowski et al. (2018) found that the contribution from post-Jurassic sedimentary rocks averaged along the entire north-south front of the Rockies from 33.5°N to 44.5°N was about 400 m of surface uplift, but the thickness of sedimentary rocks varies quite substantially from north to south. Spencer (1996) had estimated 1 km of elevation was produced by sedimentation in Colorado's High Plains, while E. D. Humphreys et al. (2015) estimated about 500 m of elevation in northeastern Colorado from preserved sedimentation. This paper will address the role of sediments more specifically and directly between 39° and 40°N latitude.

For this work, we seek to shed light on the feasibility of these uplift hypotheses by determining how much topography in the High Plains remains after observable processes are considered. Some amount of the topography in the High Plains can be accounted for by observable processes such as sedimentation and flexural response. We use the term *cryptic topography* to describe the amount of topography that remains unexplained. By attempting to quantify the amount of topography from sedimentation and flexural response, we directly address the hypothesis of Mitrovica et al. (1989): subduction-related subsidence created accommodation space for sedimentary deposits and that the thickness of the post middle Cretaceous sediments, as well the flexural, isostatic response to their emplacement, accounts for the modern topography of the High Plains. In addition, we provide baseline information that can constrain other hypotheses for the uplift of the Plains.

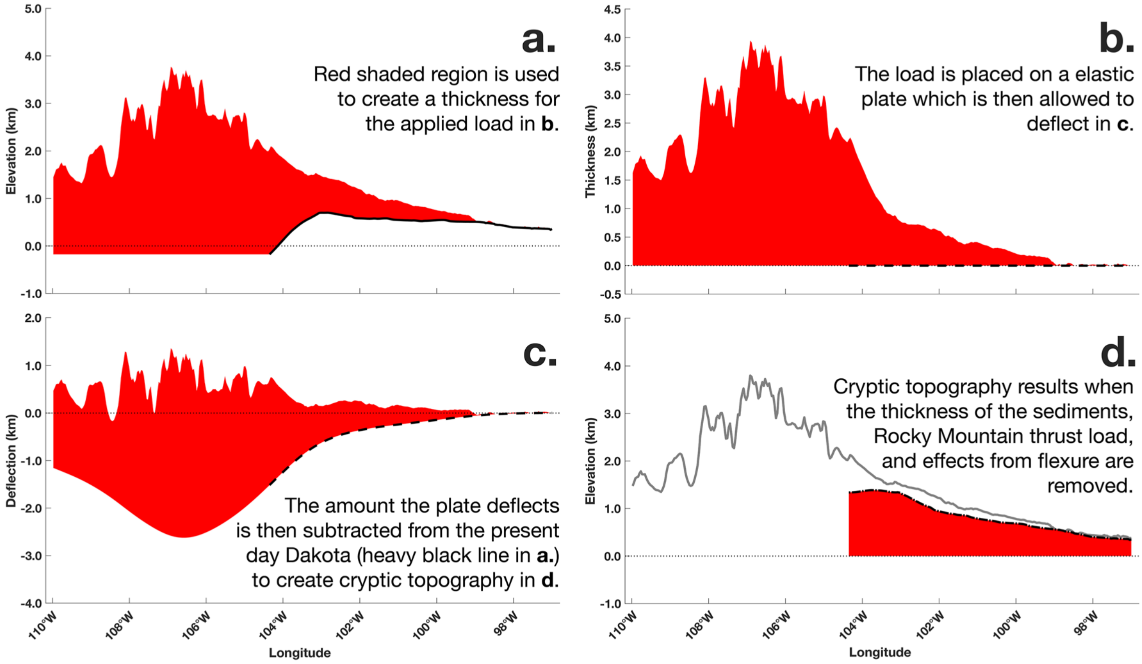

Figure 2. Schematic diagram showing that basic process for modeling the removal of the sediment and Rocky Mountain load. Heavy solid black line indicates present day horizon of the top of the Dakota. Heavy dashed lines indicate the model of the top of the Dakota as a reference surface. Heavy dashed-dotted black line in panel (d) represents cryptic topography. Heavy gray line in panel (d) represents present day surface topography, surface topography is also shown in panel (a) as the top of the red shaded region. Red shaded region represents load. Light dotted line in figures on left hand column represents sea level. Light dotted line in right column represents zero thickness and zero deflection in panels (b and c) respectively.

2. Methods

2.1. Methods Overview

The Dakota Formation was deposited near sea level during the Cretaceous about 96–100 Ma during the transgression of the Western Interior Seaway across western Kansas and eastern Colorado (e.g., Roberts & Kirschbaum, 1995). Therefore the top of this formation can be used a reference surface from which to measure post-Dakota sedimentary section thickness.

We can calculate the contribution to modern topography from the presence of this sedimentary sequence by using the thickness and density of the post-Dakota sedimentary section, estimates of the flexural rigidity of the lithosphere, and estimates of the magnitude of the Rocky Mountain load to the west of the High Plains. By modeling the lithosphere as a thin elastic plate, we can calculate the amount these factors cause a flat surface to deflect as thrust faults and sedimentation add material to the top of the Dakota Formation. We can then subtract this deflection from the present-day Dakota horizon to obtain our cryptic topography. This process is illustrated schematically in Figure 2.

First, we determine the thickness of the material overlying the Dakota in the High Plains by finding the depth to the present-day Dakota (Figure 2a). Then, we integrate the density of the rocks overlying the Dakota to calculate the total load placed on a flat reference surface representing the Dakota of Cretaceous times (Figure 2b), assuming the relief on the Dakota at the time of its deposition was negligible. Then, we model the flexural deflection of the reference surface subjected to such a load (Figure 2c). We can then subtract the effects of the flexural deflection from the modern Dakota topography to determine the amount of cryptic topography that remains to be explained. That is, the dashed line in Figure 2c is subtracted from the solid line in Figure 2a to generate the cryptic topography shown in Figure 2d. Cryptic topography amounts were calculated for three east-west profiles across eastern Colorado and western Kansas at latitudes 40°N, 39.5°N, and 39°N (Figure 3). The choice to use three east-west profiles as opposed to a 2D deflecting plate was made to simplify the deflection calculations and sensitivity analysis which are discussed later in the text along with caveats to these choices. Additionally, we are considering only the cumulative effects of the sediment emplacement and erosion since the Dakota Formation

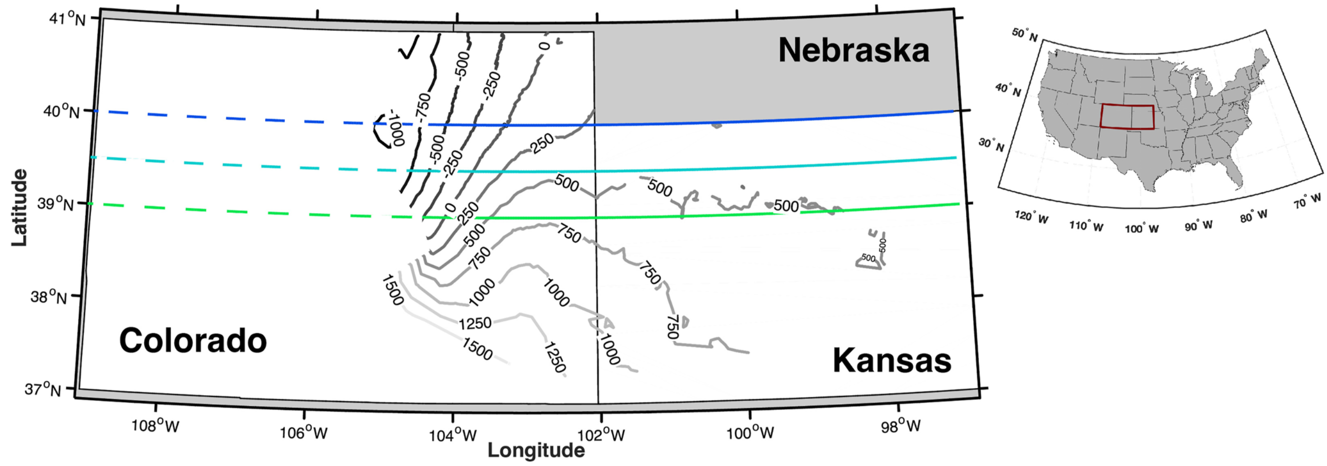

Figure 3. Map of study area. Contour lines show present day elevation in meters of the top of the Dakota relative to sea level derived from analysis of well logs. Blue, cyan, and green lines represent profiles at 40°N, 39.5°N, and 39°N. Dashed section of lines shows approximate parts of the profile where the thrust load is located. Solid section of the lines shows approximate location where Dakota Formation is found in well logs under the High Plains.

was deposited and attempting to reverse those only, thus we are not addressing any time dependent or dynamic effects, assuming that those are second-order.

2.2. Thickness and Density of Post-Cretaceous Sediments

The first step to this process is to determine the present-day elevation of the top of Dakota Formation. The difference between the present-day surface and Dakota elevation provides us with the thickness of the sediment load on the High Plains. Well logs from the Colorado Oil and Gas Conservation Commission (COGCC) as well as the Kansas Geological Survey (KGS) contain values for the depths to various formations, including the Dakota (COGCC, 2016; Kansas Geological Survey, 2016). We used 11,000 of the 20,000 well logs examined, rejecting duplicates and outliers, to map the present-day structure of the Dakota in eastern Colorado and western Kansas (Figure 3).

For each of our east-west profiles, we used wells within ±0.1° of latitude of the profile to create a 2D Dakota surface using a cubic interpolation function. We extracted the present-day elevation of the top of the Dakota from the interpolated surface along the profile line. An example of a profile with the surface elevation and the Dakota horizon is show in Figure 4. We then determined the thickness of the sedimentary load to be the difference between the surface elevation and the Dakota elevation along the profile.

Densities of the sedimentary rocks as a function of depth were made by digitizing a selection of well logs. In order to account for the contrasting geology between the Rocky Mountain and the Great Plains, the logs were divide into a subset of *mountains* and *plains* wells (Text S1 and Figure S1 in Supporting Information S1). To make reasonable estimates of the density, the data from each subset of wells, the mountain and plains wells, were fit to the function,

$$\rho(z) = \rho_{\max} - (\rho_{\max} - \rho_0)\, e^{-(z/z_c)} \tag{1}$$

where ρ_0 represents the density at the surface and $\rho_{\max}$ represents the density as $z \rightarrow \infty$ (Athy, 1930; Maxant, 1980). The fit was constrained such that the density must increase with depth, ρ_0 must exceed 1,800 kg/m^3, and $\rho_{\max}$ may not exceed 3,330 kg/m^3. Note that depth represents present day depth below the surface. The values for the parameters in density fitting function are shown in Table S1 in Supporting Information S1.

The density data and the fits of density as a function of depth are shown in Figure 5. The digitized density data are very scattered with a root mean squared deviation (RMSD) for the mountains data of 105 kg/m^3 and for the plains data of 95 kg/m^3. Because of this scatter, Figure 5 shows the well log density data points as a heat map showing the concentration of data points rather than the points themselves. In addition to the fit of the density at depth points, Figure 5 also shows the fit ±RMSD as dashed lines. To explore the effects the uncertainty in

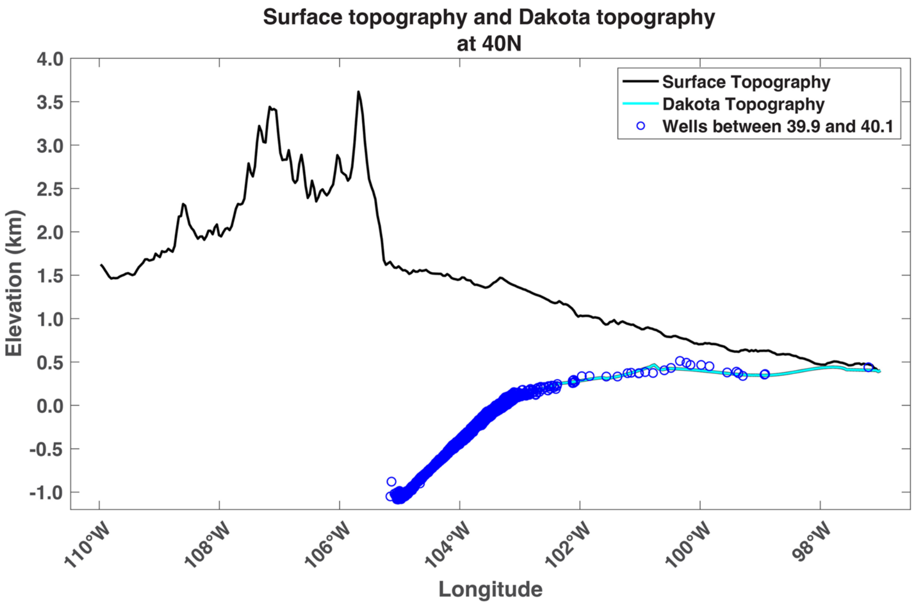

Figure 4. Profile along 40°N showing the present-day surface elevation, the present-day Dakota topography, and the well data points used in the interpolation to find the Dakota topography.

the density function had on the final calculations, we used all three of these fit lines (the preferred fit and the preferred fit ±RMSD). Thus, the force of our distributed loads can be calculated by integrating these density functions over the thicknesses of the loads.

2.3. Flexural Rigidity

The deflection of the Dakota under the weight of the overlying sediment and Rocky Mountain load is also influenced by the flexural rigidity of the lithosphere. For this work, we used three different flexural rigidity values obtained from two different sources.

We obtained two estimates for flexural rigidity by modeling the Denver Basin as a foredeep basin. The Paleogene Denver Basin initially formed during the Laramide orogeny filling with sediments from denudation of the rising Rocky Mountains (Raynolds, 2002). To determine the shape of the Denver Basin, we again used the COGCC well log database to find the depth to the top of the Fox Hills Formation, an Upper Cretaceous nearshore sandstone considered to immediately predate the Laramide uplift of the Front Range around 70 Ma (Raynolds, 2002).

A foredeep basin's shape can be modeled using an analytical solution to the thin elastic plate flexure equation. If it is assumed that the lithosphere is unbroken, that is that the slope of deflection at the point of maximum deflection is 0, the solution to the flexure equation with a line load at $x = 0$ and a distributed load representing sediment of uniform density filling the deflecting part of the elastic plate takes the form of,

$$w(x) = w_0 e^{-(x/\alpha)} \left(\cos\frac{x}{\alpha} + \sin\frac{x}{\alpha} \right) \tag{2}$$

where $w(x)$ is the deflection of the plate, w_0 is the maximum deflection (at $x = 0$), and α is the flexural parameter (e.g., Turcotte & Schubert, 2014). The flexural parameter is related to the density of the basin fill, the density of the mantle, and the flexural rigidity of the crust by

$$\alpha = \left[\frac{4D}{(\rho_\mathrm{m} - \rho_\mathrm{f})\, g} \right]^{1/4} \tag{3}$$

where D is the flexural rigidity of the crust, ρ_m is the density of the mantle, and ρ_f is the density of the sediments that fill the deflection. In all our flexural modeling we use a mantle density of 3,300 km/m^3.

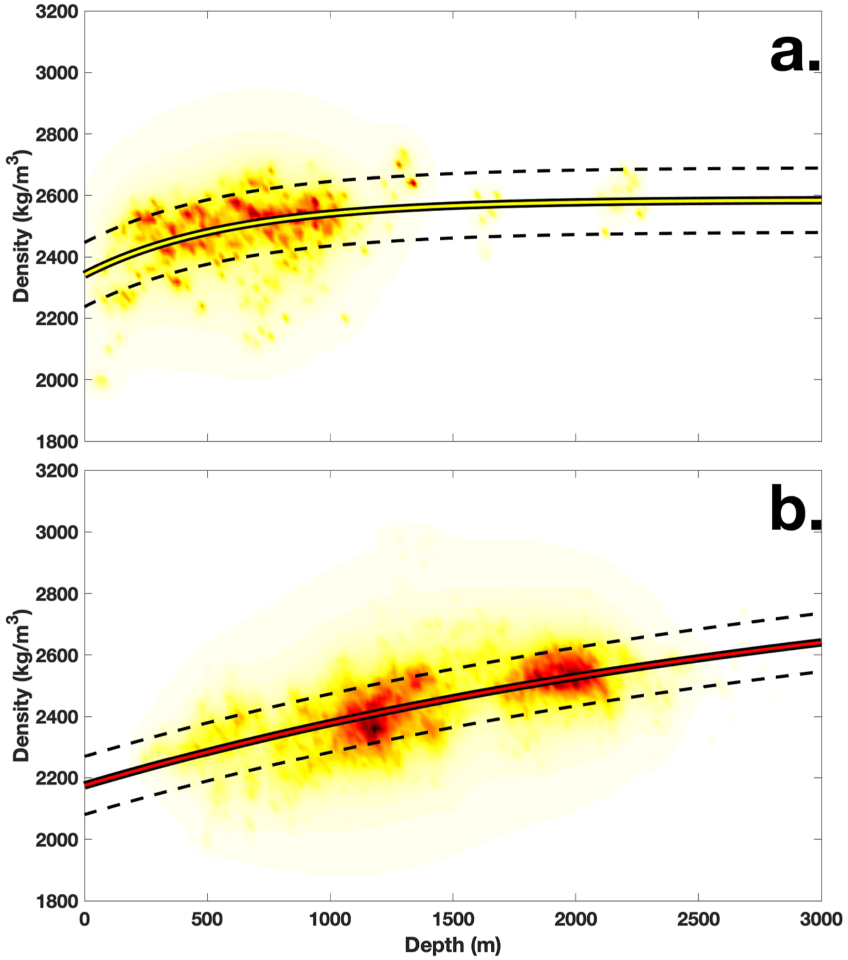

Figure 5. Heat map of data and fitting functions for density with respect to depth. Heavy colored line represents the preferred fit to the data. Dashed lines represent the preferred fit ± root mean squared deviation of the data to the fit curve. (a) Data and fitting function for the mountain data set. (b) Data and fitting function for the plains data set.

The flexural parameter also governs the wavelength of the deflection, and thus the distance of the forebulge from the line load approximating the thrust load is directly proportional to α. The flexural parameter α is also related to the distance from the point of maximum deflection to the point of zero-deflection, x_0, by $x_0 = \frac{3\pi}{4}\alpha$. Therefore, if we can determine a horizontal position of maximum deflection and a location of zero deflection, we can calculate a value for α and therefore flexural rigidity. Using this model we made two estimates of flexural rigidity described in detail in Text S2 in Supporting Information S1. The choice of using three profiles instead of a 2D deflecting plate means that these wavelengths may be only representing an east-west component of a wavelength that may have a north-south component as well and therefore are lower bounds on the flexural rigidities.

We used another set of flexural rigidities based on the work by Lowry and Pérez-Gussinyé (2011) described in Text S3 in Supporting Information S1. The Lowry and Pérez-Gussinyé (2011) flexural rigidities are derived using a different technique than our methods: that of stress balancing modern day topography and gravity measurements, thus reflecting a present-day state of flexural rigidity. The Lowry and Pérez-Gussinyé (2011) flexural rigidities are significantly higher than those we calculated. Using the mantle density and average fill density in our own flexural rigidity we calculated that the α associated with their flexural rigidities were between ~140 and 160 km. This wavelength means the distance from the point of maximum deflection to the point of zero deflection is ~330–385 km putting the point of zero deflection for the Denver basin ~75–130 km east of the Colorado-Kansas border. This appears to be unrealistically far given the absence of Denver Basin strata more than ~300 km east of the front of the Rocky Mountains and the omission of Fox Hills and upper Pierre strata to

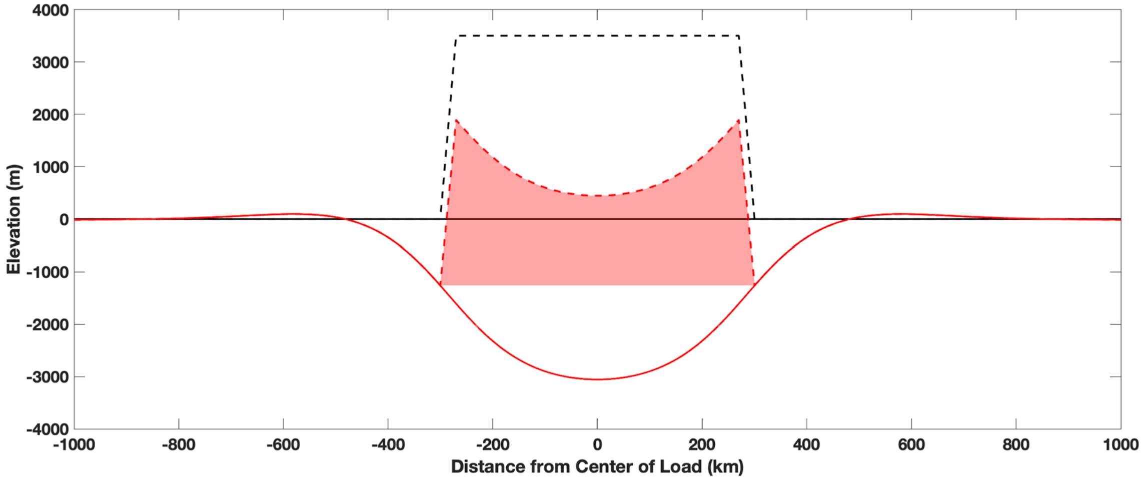

Figure 6. Example of a surface deflecting under a rectangular load. Solid black line represents the un-deflected reference surface. Dashed black line represents the geometry of the load. Solid red line represents the surface deflecting under the load. Red dashed line represents the vertical displacement of the applied load when the surface supporting it was deflected. Red shaded region illustrates the method for determining the load geometry discussed in the text.

the east. Thus, we view these flexural rigidities as upper bounds on the flexural rigidity of the lithosphere in this region during Denver Basin deposition.

2.4. Load Geometry

In the High Plains, we used the top of the Dakota as a reference surface and the thickness of the overlying sediment load is taken to be the difference in the surface elevation and the Dakota elevation. However, due to uplift and thrust faulting, the Dakota is deformed and often absent under the Rocky Mountains and therefore cannot be used as a reference surface. Much of the rock that was thrust-faulted to create the Rocky Mountains has since been eroded and Precambrian rocks that formerly underlaid the Dakota are now at the surface. Therefore, one method to estimate the thickness of the load is to simply use the difference between the present-day surface elevation of the mountains and the present-day elevation of the Dakota in the adjacent basin. If the Rocky Mountain thrust load was the only factor that was causing the Dakota to deform, this geometry likely represents an underestimate of the load, which can be illustrated by examining a simple test case scenario.

Figure 6 illustrates a case where a simple trapezoidal load is set upon a horizontal surface and the surface is then allowed to deflect. By using the methodology described in the previous paragraph, we would estimate the load to be the red shaded region. This underestimates the true geometry of the load because it doesn't account for the area between the base of the red shaded region and the deflected surface, which was part of the original trapezoid shaped load.

To account for how the uncertainty of the Rocky Mountain load affects the calculations of cryptic topography, four different estimates of the load geometry were used. In addition to the load geometry described above, three other lower boundaries for the load were used, and all four lower boundaries are shown in Figure 7. In Figure 7, Load 2 (in green) is the case where the base of the load is defined as a horizontal line extended west under the Rockies from the deepest depth of the top of the Dakota, previously explained and shown in Figure 2a.

To correct for the underestimate of the load in Load 2 as discussed above for a hypothetical trapezoidal load, Load 1 (red, Figure 7) is a load that is 1.2 times the thickness of Load 2. The lower base shown for Load 1 is determined by subtracting this thickness from the surface topography. We estimated from the exercise shown in Figure 6 that the total geometric area of the original trapezoid was ~1.5 times the size of our estimated area given the method described above. However, a load that is 1.5 times the area of the trapezoid produces unrealistically large deflections near the Rocky Mountain Front, particularly when paired with low flexural rigidities. Given that some amount of the original load size was also likely lost to erosion, a value of 1.2 was chosen instead, to estimate a more plausible maximum load size. While our estimate of a factor of 1.2 is approximate, we will show through sensitivity analysis that the value of this parameter only has limited effects on the final calculations.

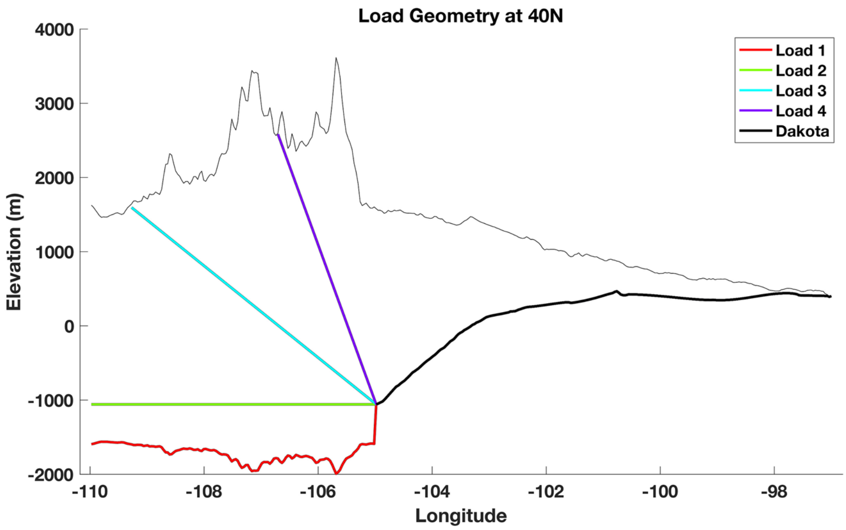

Figure 7. Illustration of the base of various Rocky Mountain load geometries. Colored lines represent the base of each load under the mountains. Heavy black line shows the Dakota horizon. Light black line shows the surface topography. Load thickness is the difference between the surface topography and the heavy lines.

Our final two loads are lower end member estimates. Load 3 (cyan, Figure 7) has a base line that connects the deepest part of the Dakota to the surface on the western side of the Rocky Mountains where the surface elevation is similar to the surface elevation above the deepest part of the Dakota. Load 4 (purple, Figure 7) extends down to a line that connects the deepest part of the Dakota to a surface outcrop of Dakota found along the profile (Nesse, 2006).

2.5. Numerical Modeling

A general version of the differential equation describing elastic plate flexure that allows for variation of density of the fill and of the flexural rigidity along the plate can be written as

$$\frac{d^2}{dx^2}\left(D\frac{d^2w}{dx^2}\right) + \rho_{\mathrm{m}} g w(x) = q(x) \tag{4}$$

where $q(x)$ is an applied load. By using a finite difference approximation, this differential equation can be solved for $w(x)$ numerically (e.g., Chapman, 2015). Thus, for a given flexural rigidity and applied load, we can calculate the amount the reference surface deflects under the load (Figure 2c). We then subtract this deflection from the present-day Dakota topography and the result is the cryptic topography.

In summary, we used three different density-depth functions, three different flexural rigidities, and four different load geometries (load thicknesses) to calculate the elastic flexure of a horizontal surface (Figure 2c). By using each possible combination of these three parameters, we calculated 36 different deflections along each of our profiles. This provides us with a range of reasonable cryptic topographies and the ability to examine the sensitivity of the cryptic topography to each of the three parameters.

Table 1
Range of Cryptic Topographies Along Each Profile

	40.0°N	39.5°N	39.0°N
West—Longitude	−104.98	−104.56	−104.35
West—Minimum	621	887	1,046
West—Mean	1,032	1,131	1,413
West—Maximum	1,531	1,464	1767
East—Longitude	−97.0	−97.0	−97.0
East—Minimum	380	335	314
East—Mean	409	375	344
East—Maximum	427	394	363

Note. Shows the minimum, maximum, and mean values for cryptic topography at the western and eastern ends of each profile. Except for the longitudes, all values given in meters.

3. Results

3.1. Cryptic Topography

The cryptic topography resulting from removing the effects of sedimentation and the Rocky Mountain thrust load are summarized in Table 1, Figures 8 and 9. Table 1 lists the maximum, minimum, and mean values of cryptic

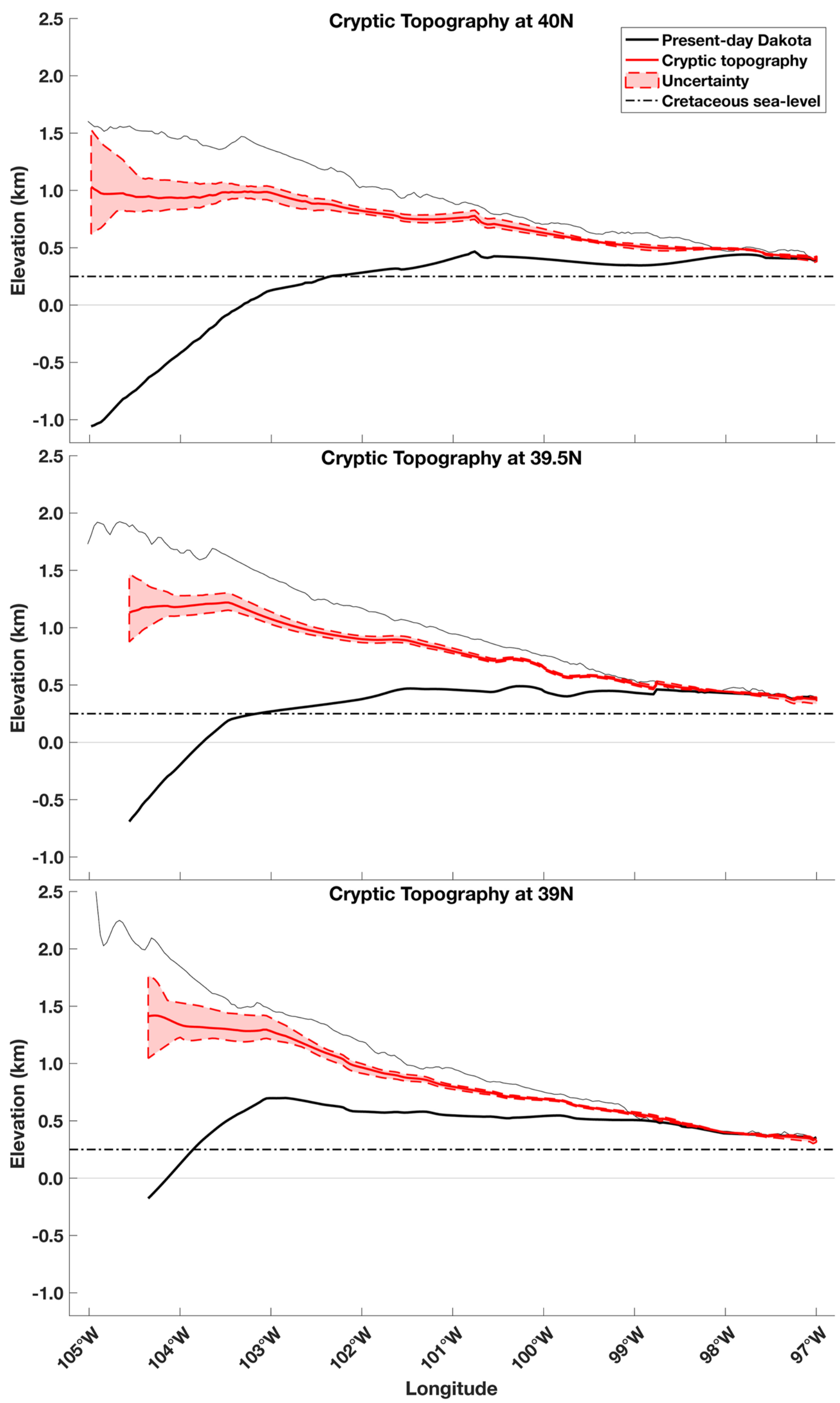

Figure 8. Cryptic topography along each profile. Dashed red lines and red shaded region represent limits of topography given variations in parameters. Heavy red line shows the average of all cryptic topographies calculated, representing preferred cryptic topography models. Cretaceous sea-level shown at 250 m above present day sea-level. Heavy black line shows present day Dakota horizon. Light black line shows present day surface topography.

topography on the western and eastern ends of each profile. Similarly, Figure 8 shows the mean value of all cryptic topographies calculated as a solid line and the full range of values from maximum to minimum as a shaded region. Figure 9 is a contour map of the mean values for cryptic topography based on all three profiles. These results indicate that the cryptic topography is higher toward the west and south. Although there are indications

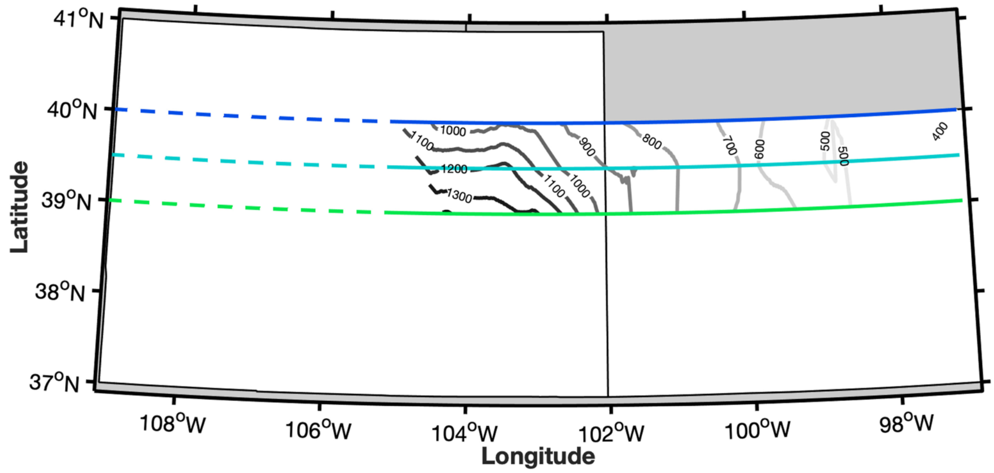

Figure 9. Topographic map of cryptic topography.

that a bend in the Dakota likely related to the thrust loading is not fully removed, leaving a slight bend in the cryptic topography profiles, particularly in the 39.5°N and 39.0°N profiles, the overall pattern is of a broad, relatively planar, dipping surface.

3.2. Sensitivity Analysis

We also seek to isolate the sensitivity of the cryptic topography to each of the three primary parameters of these calculations: the density of the sedimentary rocks, the flexural rigidity of the lithosphere, and the geometry of the thrust load of the Southern Rockies. To do this, we plotted the range of cryptic topography with two of the parameters held constant and varying the third parameter over the full range of uncertainty as described above.

To examine the sensitivity of the cryptic topography to density, we calculated three different cryptic topography profiles from a single value of flexural rigidity (the higher estimate of the two from our Fox Hills modeling), a single load geometry (Load 3, shown in cyan in Figure 7), and the three different density-depth profiles in Figure 5, one where the best-fit curve is used, one where the lower density fitting curve is used, and one where the higher density fitting curve is used. Figure 10a shows the sensitivity of cryptic topography to density for the 40°N profile. Figure 10a illustrates that on the westernmost side of the profile, the different density fitting functions only created about 165 m in spread in the uncertainty of cryptic topography on this profile. The higher density functions produce more deflection of the Dakota and therefore result in greater cryptic topography. There was similar uncertainty for the other two profiles with 141 m of variation on the 39.5°N profile and 118 m on the 39°N profile. This uncertainty was not sensitive to the other parameters of flexural rigidity and density fitting function.

A similar sensitivity analysis was done to evaluate the effects of the flexural rigidity value on the cryptic topography. Figure 10b shows a subset of cryptic topographies for the 40.0°N profile in which a single load geometry (again, Load 3 shown in cyan in Figure 7) and a single density fitting function (the preferred fit, or heavy colored lines in Figure 5) were used with three different flexural rigidity values: the two from our modeling of the Fox Hills deflection and one from Lowry and Pérez-Gussinyé (2011). Like the last sensitivity test, the variation in flexural rigidity only created a maximum of 154 m of variation in the cryptic topographies on the 40°N profile. The 39.5°N and 39°N had 81 and 198 m of variation in cryptic topographies, respectively. The different flexural rigidity values impact the shape of the deflection as well as the amount. For higher flexural rigidity, the plate is stiffer and wavelength of the plate bending increases. This results in making our cryptic topography a little higher near the Rocky Mountain Front and lower farther east on the Plains, but generally flatter across the region. Once again, these ranges in variation are similar to values made using other choices for load geometry and density fitting function.

The final sensitivity analysis was done for the load geometry. Figure 10c shows a subset of cryptic topographies along the 40.0°N profile in which a single value of flexural rigidity (again, the higher estimate of the two from our Fox Hills modeling) and the preferred density fitting function were used with all four different load geometries

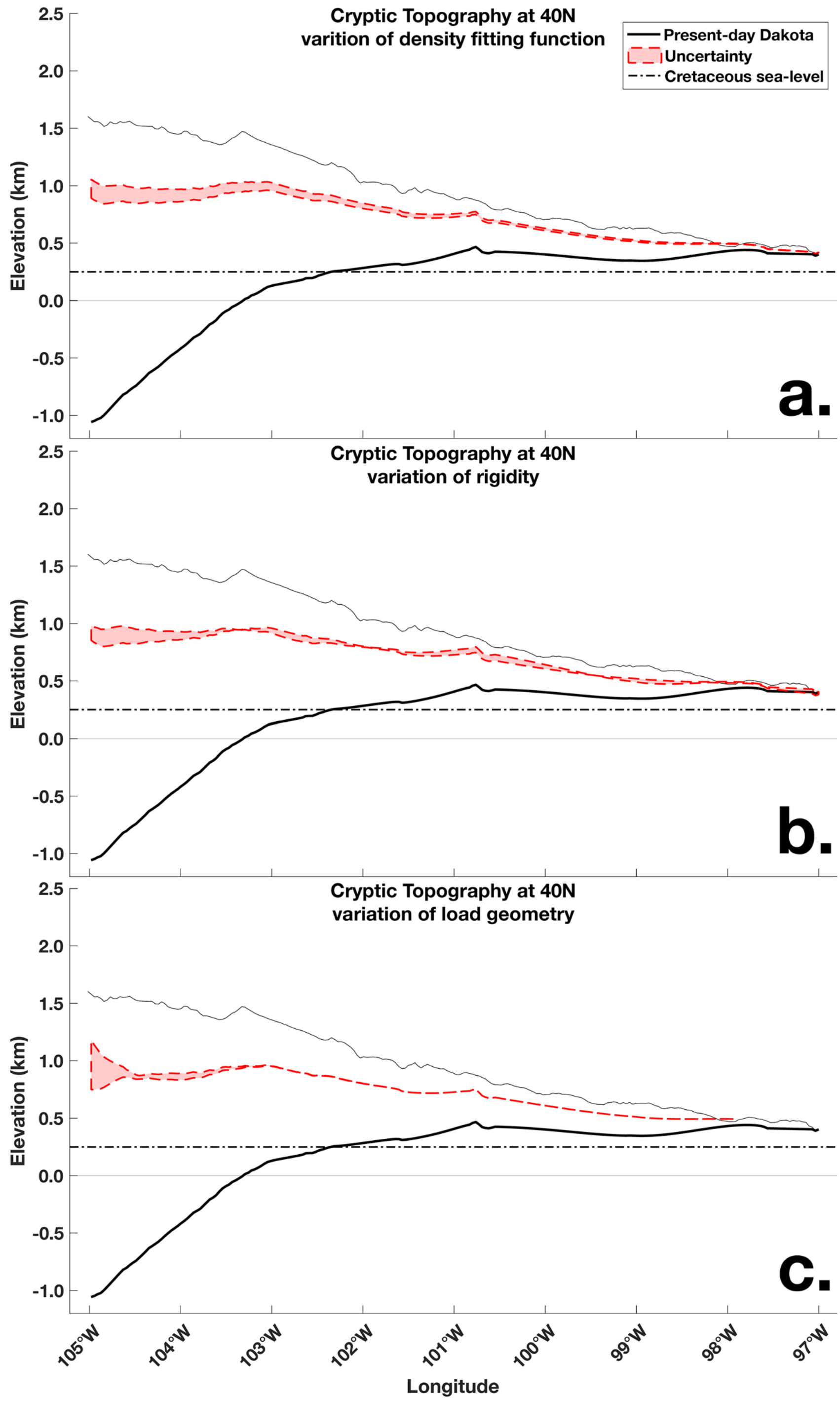

Figure 10. Plots of different subsets of cryptic topographies along 40.0°N profile. (a) Only the density fitting function changes between the different cryptic topographies. (b) Only the flexural rigidity changes between the different cryptic topographies. (c) Only the geometry of the Rocky Mountain load changes between the different cryptic topographies.

(shown in Figure 7). Of the three different parameters, the range of values we used for load geometry added the greatest maximum amount of uncertainty to cryptic topography across the profile. The largest amount of variation on the 40.0°N profile was 431 m, for the 39.5°N profile it was 379 m, and for the 39.0°N profile it was 415 m. As expected, larger load sizes resulted in greater deflection on the Dakota and therefore higher cryptic topography. However, Figure 10c also shows that the upper and lower limits of cryptic topography flare out only over a short distance (~60–80 km) at the western edge of the profile. This increased uncertainty does have a slightly different wavelength depending on what flexural rigidity is used, but that uncertainty is still mostly confined to the 60–80 km range on all three profiles.

4. Discussion

Even with the uncertainties in our calculations, our cryptic topography profiles indicate between 1,000–1,500 m of topography in the High Plains cannot be explained by post-middle-Cretaceous sedimentation and thrust loading of the Rocky Mountain front. Given that Cretaceous sea-level was higher than present day (about 250 m, e.g., Sames et al. (2016)), this leaves between 750 and 1,250 m of unexplained or cryptic topography. Our analysis limits the extent that the hypothesis by Mitrovica et al. (1989) explains the present day topography of the High Plains as resulting from the deposition of Cretaceous sediments in a trough created by dynamic topography that subsequently rebounded as dynamic subsidence ended. That process explains no more than half of the present elevations of the High Plains at these latitudes.

Our estimate of ~1 km of cryptic topography in the High Plains is notably consistent with the conclusion of Levandowski et al. (2018) who predicted 900 m of elevation in the western High Plains as well as the eastward decrease in elevation could be explained by crustal density patterns, consistent with the crustal hydration hypothesis proposed by Jones et al. (2015). It is higher by about a factor of two than inferred by Spencer (1996), who assumed a full 3 km of sediment was responsible for 1 km of elevation in the western Great Plains. Our estimate of the contribution from sedimentary rocks is very similar to an estimate from E. D. Humphreys et al. (2015) that covered a much broader region. Neither Spencer (1996) nor E. D. Humphreys et al. (2015) addressed the possible impact of thrust loading on sediment preservation.

We now consider the constraints our cryptic topography places on possible hypotheses for producing this elevation. The principal spatial pattern in our result is a broad west-to-east decrease in cryptic topography along with a north-to-south increase within Colorado (west of ~102°W) (Figure 9). Although most of the north to south increase coincides with higher elevations associated with preserved early Tertiary rock on the Palmer Divide, the inclusion of that load in our flexural profile actually makes our estimate of cryptic topography somewhat lower than a fully 2-D analysis would produce. We think that higher amount of cryptic topography in the south is present in a topographic profile at 38°N, where the Dakota Formation is at or near the Earth's surface and thus the topography is very close to our cryptic topography. That profile's similar or slightly higher elevations than our 39° profile despite being along the Arkansas River valley supports the north-to-south variation as real.

As noted in the introduction, a number of possible means of creating surface uplift since the Cretaceous have been proposed. We have explicitly removed the contribution from the elevation-through-sedimentation idea of Mitrovica et al. (1989). We subdivide remaining hypotheses by their first-order geographic characteristics: slab-related, magmatic, rift-related, and dynamic topography. Slab-related mechanisms include physical removal of lithosphere (Smith, 2010; Spencer, 1996) crustal hydration (Jones et al., 2015) and mantle hydration (E. Humphreys et al., 2003). These will depend on the exact geometry of the Laramide age slab, but effects should decrease with distance from either the trench or the first contact of the slab top with asthenosphere. Magmatically derived uplift has been envisioned to result from iron depletion associated with the creation of large volume, high-silica igneous centers including the San Juan volcanic field in southwestern Colorado and the Mogollon-Datil field near the Arizona-New Mexico border. This effect would presumably extend outward from these volcanic centers and so predicts a greater effect to the south than to the north. Rift-related uplift would mostly reflect mechanical and/or thermal thinning of mantle lithosphere, but in this case the greatest thinning would be along the Rio Grande Rift and decrease away from there. Predictions from dynamic topographic models depend on the model but must integrate over the past c. 80 Ma; the model of Liu and Gurnis (2010) satisfies this requirement.

Figure 11 compares several qualitative predictions of spatial surface uplift patterns from these different hypotheses to the contour lines of cryptic topography shown in Figure 9. Figure 11a shows a pattern of uplift loosely based on the hypothesis of Roy et al. (2004, 2005) in which Tertiary magmatism is at least partially responsible for surface uplift. In this panel, the greatest amount of uplift is focused around the San Juan Volcanic Field (Farmer et al., 2008). Figure 11b shows the pattern of uplift estimated for uplift associated with upwelling associated with the Rio Grande Rift. If the rift extends farther north into the state of Colorado the area of maximum uplift may also extend farther north, but we might still expect an overall decrease in uplift to the north. Figure 11c

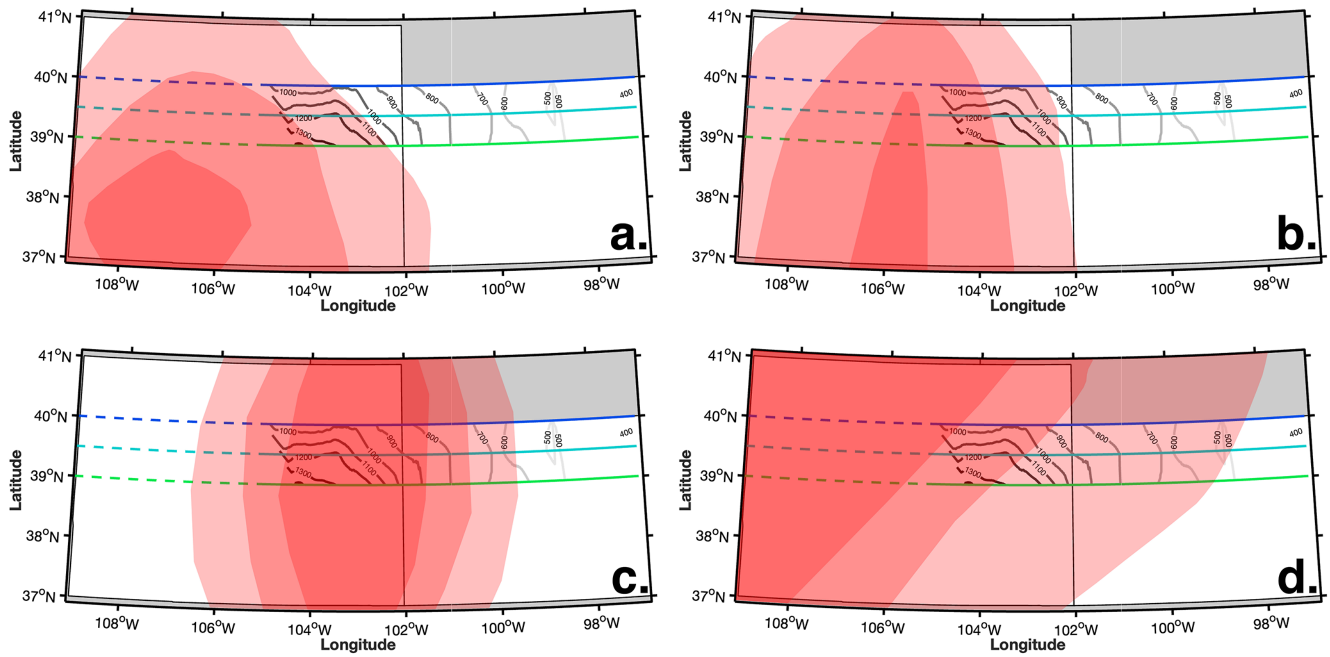

Figure 11. Maps showing predicted qualitative uplift patterns and contour lines of cryptic topography. Shaded red regions show estimates relative amounts of predicted uplift from various uplift scenarios with darker areas showing greatest amounts of uplift. (a) Uplift pattern from volcanism. (b) Uplift pattern from Rio Grande Rift upwelling. (c) Uplift pattern from dynamic topography from Liu and Gurnis (2010). (d) Uplift pattern from Laramide hydration using a narrow flat (or shallow) slab model.

shows the greatest uplift focused on the western plains based on the dynamic topography uplift model of Liu and Gurnis (2010). For this prediction, the contours are based on subtracting their predicted dynamic topography of 100 Ma from the present day predicted dynamic topography, thus determining how much the topography has changed as a result of dynamic processes since 100 Ma. Figure 11d shows an uplift pattern in which the greatest areas of uplift are focused above a narrow flat or shallowly subducting slab as envisioned by Saleeby (2003). This uplift pattern could result from crustal and/or mantle hydration resulting from the shallow slab. Note that a different slab geometry (e.g., that of Bird, 1984) would make a different prediction.

The limited extent of our estimate of cryptic topography makes testing these hypotheses against our inferences challenging to evaluate, but the spatial pattern, which decreases to the north and east, appears to be most consistent with magmatism focused on the San Juan Volcanic Field or rift upwelling. The uplift pattern from dynamic topography shows some correlation with our contour lines of cryptic topography, however we see a more rapid decrease in cryptic topography northward than the predicted uplift patterns. The cryptic topography contour lines do not match up particularly well with the narrow slab uplift pattern but might be more consistent with a slightly different incidence angle for the slab. The great extent of cryptic topography to the east, though, probably demands at least some component from slab-related mechanisms or possibly dynamic topography.

The final cryptic topography increases in elevations to the south. If this pattern were to continue farther south of our three profiles, this would have broad implications for what types of hypotheses can explain the High Plains. Adding additional profiles to the north and south would shed light on this pattern but also introduce new challenges. To the south, the Dakota is increasingly shallower, and by the New Mexico border erosion has removed any overlying strata and eaten into the Dakota itself.

Constraining the timing of the uplift of the High Plains would help constrain the mechanism for uplift. The general east dipping slope of our cryptic topography is similar to the 1 m/km tilt attributed to regional tilting in the last 5 Ma predicted by Riihimaki et al. (2007). If our cryptic topography has formed this recently, this timing is also consistent with the 500 m of dynamic topography generated by removal of mantle lithosphere under the Colorado Plateau proposed to have occurred in the last 10 Ma by Moucha et al. (2008), although mantle lithosphere removal is not evident in the High Plains seismic tomography (Shen et al., 2013).

5. Conclusions

In this paper, we sought to quantify the amount of topography in the High Plains that could be explained by the sedimentation and thrust loading of the Rocky Mountains. To do this, we calculated the effects that the emplacements of these loads would have on a flexural plate and subtracted those effects from the modern topography. We did this by estimating the force applied by this load based on its thickness and density provided by well log data, and the flexural response of the lithosphere to that load.

After testing the sensitivity of our methods to our assumptions and the uncertainties in the data, we determined that the cryptic topography is a broad, relatively planar surface that dips slightly to the ENE. Its maximum elevation is 1.5 km at the western edge of our southernmost profile at 39°N, and closer to 1 km on the western edge of our northernmost profile at 40°N. This amount of unexplained topography shows that the present-day elevation of the High Plains cannot be explained by sedimentation and thrust loading alone, and it provides a constraint on the amount and geometry of topography that was created from other processes.

Data Availability Statement

The well log data used for the depth to the Dakota Formation and the Fox Hills formation as well as the density logs in Colorado are available from the Colorado Oil and Gas Conservation Commission at https://cogcc.state.co.us/data.html#/cogis where individual wells can be searched. We used original Matlab scripts to search through every well log available at the time to find depth to the Dakota Formation top, depth to Fox Hills top, and density logs. Information for individual wells can be found by modifications to the URL https://cogcc.state.co.us/cogis/FacilityDetail.asp?facid=XXXXXXXX%26type=WELL where XXXXXXXX can be replaced with a Well API using leading zeros to ensure each API is eight characters. The depth to formation tops are found on these information pages as well as a link called "Doc" which leads to well documentation available including density logs. We have included files "Fox Hills Well APIs" (Data Set S1) and "Dakota Formation APIs" (Data Set S2) in Supporting Information which contain lists of the APIs for wells used to map the tops of each of these formations as well as the relevant information used to establish a present day elevation for each formation. There is also a file "Density Data Well APIs" (Data Set S3) listing the well APIs for the density well logs we digitized for this work. The well log data used to find the depth to the Dakota Formation in Kansas are available from the Kansas Geological Survey at https://www.kgs.ku.edu/PRS/petroDB.html. At the bottom of this page, the file ks_tops.zip contains the data used in this report. Since this format contains all the well tops in Kansas, we have included a file "Dakota Formation—Kansas" (Data Set S4) in Supporting Information that contains only the well tops to the Dakota formation in a file that the Kansas Geological Survey provided at the time the data was accessed. They no longer provide well tops for specific formations on their website.

Acknowledgments
We would like to thank Matt Weingarten for assisting with accessing well log data in Colorado. We also would like to acknowledge NSF EAR-1547123 for providing support for much of this project duration. Also thanks to Karen Berry and Matt Morgan and the Colorado Geological Survey and for providing continued support for this research. This manuscript benefited from reviews from A. Lowry and E. Humphreys.

References

Athy, L. F. (1930). Density, porosity, and compaction of sedimentary rocks. *AAPG Bulletin*, *14*(1), 1–24. https://doi.org/10.1306/3D93289E-16B1-11D7-8645000102C1865D

Bird, P. (1984). Laramide crustal thickening event in the Rocky Mountain foreland and Great Plains. *Tectonics*, *3*(7), 741–758. https://doi.org/10.1029/TC003i007p00741

Chapman, J. (2015). Flex2D [Matlab]. Retrieved from https://www.jaychapman.org/matlab-programs.html

COGCC. (2016). Retrieved from https://cogcc.state.co.us/data.html%23/cogis

Davis, G. H. (1999). *Structural geology of the Colorado Plateau region of southern Utah, with special emphasis on deformation bands*. Geological Society of America Special Papers (Vol. 342, pp. 1–157).

Farmer, G. L., Bailley, T., & Elkins-Tanton, L. T. (2008). Mantle source volumes and the origin of the mid-Tertiary ignimbrite flare-up in the southern Rocky Mountains, western U.S. *Lithos*, *102*(1–2), 279–294. https://doi.org/10.1016/j.lithos.2007.08.014

Humphreys, E., Hessler, E., Dueker, K., Farmer, G. L., Erslev, E., & Atwater, T. (2003). How Laramide-age hydration of North American lithosphere by the Farallon slab controlled subsequent activity in the western United States. *International Geology Review*, *45*(7), 575–595. https://doi.org/10.2747/0020-6814.45.7.575

Humphreys, E. D., Schmandt, B., Bezada, M. J., & Perry-Houts, J. (2015). Recent craton growth by slab stacking beneath Wyoming. *Earth and Planetary Science Letters*, *429*, 170–180. https://doi.org/10.1016/j.epsl.2015.07.066

Jones, C. H., Mahan, K. H., Butcher, L. A., Levandowski, W. B., & Farmer, G. L. (2015). Continental uplift through crustal hydration. *Geology*, *43*(4), 355–358. https://doi.org/10.1130/G36509.1

Kansas Geological Survey. (2016). Retrieved from http://www.kgs.ku.edu/Magellan/Tops/index.html

Levandowski, W., Jones, C. H., Butcher, L. A., & Mahan, K. H. (2018). Lithospheric density models reveal evidence for Cenozoic uplift of the Colorado Plateau and Great Plains by lower-crustal hydration. *Geosphere*, *14*(3), 1150–1164. https://doi.org/10.1130/GES01619.1

Liu, L., & Gurnis, M. (2010). Dynamic subsidence and uplift of the Colorado Plateau. *Geology*, *38*(7), 663–666. https://doi.org/10.1130/G30624.1

Lowry, A. R., & Pérez-Gussinyé, M. (2011). The role of crustal quartz in controlling Cordilleran deformation. *Nature*, *471*(7338), 353–357. https://doi.org/10.1038/nature09912

Maxant, J. (1980). Variation of density with rock type, depth, and formation in the Western Canada basin from density logs. *Geophysics*, *45*(6), 1061–1076. https://doi.org/10.1190/1.1441107

Mitrovica, J. X., Beaumont, C., & Jarvis, G. T. (1989). Tilting of continental interiors by the dynamical effects of subduction. *Tectonics*, *8*(5), 1079–1094. https://doi.org/10.1029/TC008i005p01079

Morgan, P. (2003). Colorado Plateau and southern Rocky Mountains uplift and erosion. In R. G. Raynolds & R. M. Flores (Eds.), *Cenozoic systems of the Rocky Mountain region: Denver Colorado, Rocky Mountain SEPM* (pp. 1–31).

Morgan, P., & Swanberg, C. A. (1985). On the Cenozoic uplift and tectonic stability of the Colorado plateau. *Journal of Geodynamics*, *3*(1–2), 39–63. https://doi.org/10.1016/0264-3707(85)90021-3

Moucha, R., Forte, A. M., Rowley, D. B., Mitrovica, J. X., Simmons, N. A., & Grand, S. P. (2008). Mantle convection and the recent evolution of the Colorado Plateau and the Rio Grande Rift valley. *Geology*, *36*(6), 439. https://doi.org/10.1130/G24577A.1

Nesse, W. D. (2006). Geometry and tectonics of the Laramide Front Range, Colorado. *Mountain Geologist*, *43*(1), 25–44.

Raynolds, R. G. (2002). Upper Cretaceous and Tertiary stratigraphy of the Denver basin, Colorado. *Rocky Mountain Geology*, *37*(2), 111–134. https://doi.org/10.2113/gsrocky.37.2.111

Riihimaki, C. A., Anderson, R. S., & Safran, E. B. (2007). Impact of rock uplift on rates of late Cenozoic Rocky Mountain river incision. *Journal of Geophysical Research*, *112*(F3), F03S02. https://doi.org/10.1029/2006JF000557

Roberts, L. N. R., & Kirschbaum, M. A. (1995). Paleogeography and the Late Cretaceous of the Western Interior of middle North America; coal distribution and sediment accumulation. *USGS Professional Papers*, *1561*, 120. https://doi.org/10.3133/pp1561

Roy, M., Jordan, T. H., & Pederson, J. (2009). Colorado Plateau magmatism and uplift by warming of heterogeneous lithosphere. *Nature*, *459*(7249), 978–982. https://doi.org/10.1038/nature08052

Roy, M., Kelley, S. A., Pazzaglia, F., Cather, S., & House, M. (2004). Middle Tertiary buoyancy modification and its relationship to rock exhumation, cooling, and subsequent extension at the eastern margin of the Colorado Plateau. *Geology*, *32*(10), 925–934. https://doi.org/10.1130/G20561.1

Roy, M., MacCarthy, J. K., & Selverstone, J. (2005). Upper mantle structure beneath the eastern Colorado Plateau and Rio Grande rift revealed by Bouguer gravity, seismic velocities, and xenolith data. *Geochemistry, Geophysics, Geosystems*, *6*(10), 1–19. https://doi.org/10.1029/2005GC001008

Saleeby, J. B. (2003). Segmentation of the Laramide slab - Evidence from the southern Sierra Nevada region. *The Geological Society of America Bulletin*, *115*(6), 655–668. https://doi.org/10.1130/0016-7606(2003)115<0655:SOTLSF>2.0.CO;2

Sames, B., Wagreich, M., Wendler, J. E., Haq, B. U., Conrad, C. P., Melinte-Dobrinescu, M. C., et al. (2016). Review: Short-term sea-level changes in a greenhouse world—A view from the Cretaceous. *Palaeogeography, Palaeoclimatology, Palaeoecology*, *441*, 393–411. https://doi.org/10.1016/j.palaeo.2015.10.045

Shen, W., Ritzwoller, M. H., & Schulte-Pelkum, V. (2013). A 3-D model of the crust and uppermost mantle beneath the Central and Western US by joint inversion of receiver functions and surface wave dispersion. *Journal of Geophysical Research: Solid Earth*, *118*(1), 262–276. https://doi.org/10.1029/2012JB009602

Smith, D. (2010). Antigorite peridotite, metaserpentinite, and other inclusions within diatremes on the Colorado Plateau, SW USA: Implications for the mantle wedge during low-angle subduction. *Journal of Petrology*, *51*(6), 1355–1379. https://doi.org/10.1093/petrology/egq022

Spencer, J. E. (1996). Uplift of the Colorado Plateau due to lithosphere attenuation during Laramide low-angle subduction. *Journal of Geophysical Research*, *101*(B6), 13595–13609. https://doi.org/10.1029/96JB00818

Turcotte, D., & Schubert, G. (2014). *Geodynamics (third)*. Cambridge University Press.